Drag force of polyethyleneglycol in flow measured by a scanning probe microscope

Ruri Hidema,* Seika Hayashi, and Hiroshi Suzuki
Department of Chemical Science and Engineering, Kobe University, Kobe 657-8501, Japan

(Received 25 July 2018; published 30 July 2019)

We propose a method to measure the drag force due to synthetic polymers in flowing fluids by using a scanning probe microscope (SPM). Methoxy polyethyleneglycol thiol (mPEG-SH) was attached to the cantilever probe of the SPM, which was further immersed in flows of glycerol and polyethyleneglycol (PEG) solutions. The mPEG-SH-bonded cantilever detects the extra force due to polymer-polymer and polymer-fluids interaction in flowing fluids. The conformation of the mPEG-SH polymer bonded to the probe of the cantilever was predicted as having a stem and ellipsoidal-flower shape, and the drag force due to the deformed mPEG-SH was calculated. The forces detected by experiments using the SPM and the forces obtained by model calculations were compared and found to be reasonably close.

DOI: 10.1103/PhysRevFluids.4.074201

I. INTRODUCTION

The addition of a little amount of polymer to Newtonian fluids induces complex behaviors, such as drag reduction [1–9], elastic instabilities [10–14], and increase of extensional relaxation time or extensional viscosities [15–20]. Polymers in fluids are deformed during the flow and may interact with each other, which affects the rheological properties of the fluids. However, it is difficult to make a direct measurement of the polymer behavior in flowing fluids and, therefore, it is difficult to predict the impacts of adding synthetic polymers to the fluids.

When we focus on direct measurements of polymers' properties in fluids, an experimental technique is known to measure the mechanical properties of a single polymer chain in a resting solution. The experimental technique known as nanofishing uses an atomic force microscope (AFM) to obtain a force-extension curve of a tethered single polymer in a resting solution. By using this technique, many experimental studies have been made in the past several decades.

It has been a hot topic to elucidate the entropic and enthalpic elasticity of a single chain via the force-extension curve measured by the nanofishing. Extension curves of biopolymers and synthetic polymers were observed and used to discuss their entropic elasticity [21–26]. Two main mechanical models, the freely jointed chain (FJC) and the worm like chain (WLC) models, were utilized to describe the force-extension curves. The FJC model describes a single, isolated, flexible, polymer chain without any long-range interactions. The WLC model describes a polymer chain with intermediate behavior between a rigid-rod and a flexible coil [21,27,28]. In addition, further development of these models is still an important research topic [29]. The force extension curve was also utilized to reveal the conformational change of a single polymer chain, such as the unfolding of proteins [30,31], the elasticity switch of single photochromic macromolecules [32], and the mechanical stability of proteins in the presence of chemical reactions [33]. There are also previous studies that focus on the force extension curve in terms of the type of interaction. For example, the interaction in a polymer [34], the interaction between polymers and the solvent [35], the interaction between polymers and a substrate [36], and the polymer-nanoparticle interaction [37] are reported.

*hidema@port.kobe-u.ac.jp

Here, we focus on the dynamics of a tethered polymer in a flow, which has been studied both numerically [38–42] and experimentally [43–46]. The pioneering numerical studies of Brochard-Wyart and coworkers showed the elongation of a tethered DNA molecule under force or in flows [38,39]. They proposed three types of conformation of the DNA molecules in flows based on a uniform tension force due to the fluid velocities. The first type is an unperturbed conformation at low velocities. The second type is the "Trumpet" model that is partly stretched by certain scaling laws, which occurs at intermediate velocities. The third type is the "Stem and Flower" model, which consists of a completely stretched part and a coiled part, occurring at high velocities. Brochard-Wyart *et al.* [47] proposed an index (φ) to predict the polymer conformation. The index φ is described as follows:

$$\varphi = \frac{f l_{\mathrm{po}}}{k_{\mathrm{B}} T}, \tag{1}$$

where f is the uniform tension force applied to the polymer, l_{op} is the unperturbed persistent length, k_{B} is Boltzmann's constant, and T is temperature. When φ is greater than 1, the polymer is in a taut regime. When φ is below 1, polymer is in an unperturbed coil regime, a trumpet regime, or in a stem-and-flower regime. Rzehak *et al.* conducted a more detailed numerical simulation about the deformation of a tethered polymer in a uniform flow [40]. They calculated the distribution of free ends of a tethered polymer by taking into account the excluded-volume and hydrodynamic interactions. They predicted the tethered polymer conformation and calculated the total drag force exerted on the polymer by the external flow. The effects of the polymer length on its dynamics were also discussed [40], and it is still a hot topic to be explored [42].

Experimental studies of a tethered DNA molecule in a shear flow have been reported based on the great interest on biophysical and genomic applications, as well as on the fundamental polymer dynamics [43–46]. For instance, Fisher *et al.* visualized the DNA relaxation dynamics as a means to probe the intracellular environment [46], Perkins *et al.* stretched DNA molecules in a microchannel by applying extensional flow [43], and Ladoux and Doyle calculated the force required to stretch DNA due to shear stress based on the FJC and WLC models [44]. In these experimental studies, the polymer deformation predicted by calculating φ was confirmed.

As described above, a large number of AFM nanofishing experiments of bio and synthetic polymers in solutions were conducted, and many numerical and experimental studies describing the behavior of a tethered DNA molecule in a flow were reported. However, there are only a few experimental studies discussing the behavior of synthetic polymers in a flow [48]. This is because the size of synthetic polymers is too small to allow a proper visualization. In addition, to the best of our knowledge, no experimental study combining AFM and a flow to detect the drag force caused by polymers, especially synthetic polymers, was conducted so far.

In this study, we propose a method to measure the drag force due to synthetic polymers in a flow by using a scanning probe microscope (SPM). Polymers were attached to a cantilever probe held by the SPM, and the cantilever was further immersed in a flow. Glycerol and polymer solutions were prepared to be used as flow solutions. We measured the drag force on the cantilever probe in the flow of glycerol and polymer solutions. By comparing the drag force on the probe in several conditions, we predict the drag force due to polymers that were attached to the probe. We also predict the force due to the interaction between the attached polymers with the flow, and the force due to the mutual interaction between the polymers attached to the probe with the polymers in the flow. From now on, we call these interactions as polymer-fluids interactions and polymer-polymer interactions, respectively.

II. EXPERIMENTAL PROCEDURES

A. Materials

The glycerol (FUJIFILM Wako Pure Chem. Corp.) solutions used as Newtonian fluids were prepared in a wide range of concentrations, as shown in Table I. Polyethyleneglycol (PEG,

TABLE I. Viscosity and density of each glycerol solution.

Glycerol concentration (wt%)	Viscosity (10^{-3} Pa s)	Density (kg m^{-3})
5	1.15	1013
6	1.24	1016
8	1.32	1021
10	1.40	1026
15	1.59	1039
22	1.88	1058
35	2.41	1093

molecular weight: 20 000, FUJIFILM Wako Pure Chem. Corp.) was used as a polymer, wherein concentrations were varied as shown in Table II. The viscosity of the sample solutions was measured by using a rheometer (MCR301: Anton Paar) with a cone-plate device. The concentrations of the glycerol solutions were controlled to achieve similar viscosities to each PEG solution. The density of each solution was measured by a densimeter.

To attach polymers to the cantilever probe, methoxy polyethyleneglycol thiol (mPEG-SH, molecular weight: 20 000, Laysan Bio Inc.), which has a free thiol group at one end, was dissolved in pure water at the concentration of 1 wt%. The thiol group became bonded to the gold-coated cantilever probe, as described later.

B. Experimental apparatus to measure drag force

The experiments were performed combining the several apparatuses shown in Fig. 1(a). The main apparatus is a scanning probe microscope (SPM, Innova: Bruker Nano). A small channel was attached to the sample stage of the SPM and connected to two syringes by tubing [Figs. 1(b) and 1(c)]. A syringe was filled with sample solutions, and the flow rates of inlet sample solutions were controlled by two syringe drivers. The flow rates were varied from 2 to 5 ml/min. A whole image representation of the flow channel is shown in Fig. 1(c), while Fig. 2(d) and Fig. 4 show the lateral view of the channel. A small stainless-steel piece was sunk in the channel to stabilize the flow, producing a uniform flow at the inlet and a fully developed flow around the cantilever probe. Here we use a gold-coated cantilever probe with a V-shaped tip (Biolever, BL-RC150VB-C1, B lever, Olympus). Geometrically, it is a hollow pyramid vertically sliced in half, with a sharpened apex. The convex surface of the probe is fully coated with gold. The front view of the probe, from the convex side, is a triangle with 12 μm base and 7 μm height. An upside-down image of the cantilever illustrating the V-shaped probe, and the front view of the probe, are shown in Figs. 12(c) and 12(d), respectively. The spring constant of the probe is 6 pN/nm.

TABLE II. Viscosity and density of each PEG solution.

PEG concentration (wt%)	Viscosity (10^{-3} Pa s)	Density (kg m^{-3})
0.50	1.13	1001
0.75	1.23	1002
1.00	1.32	1003
1.25	1.39	1003
1.50	1.59	1003
2.00	1.83	1005
3.00	2.41	1008

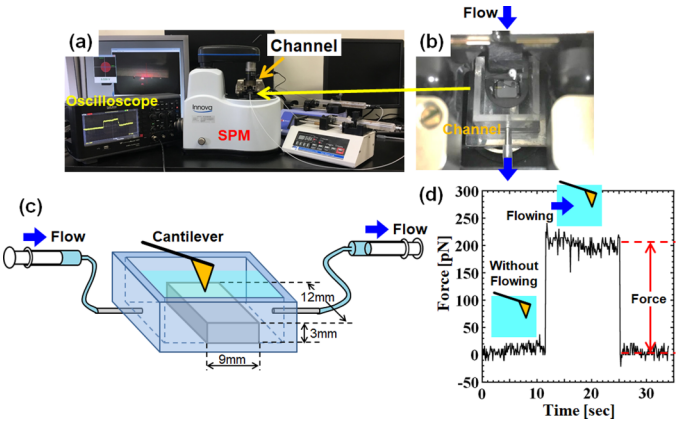

FIG. 1. (a) Whole image of the experimental setup. (b) Flow channel attached on the sample stage of the SPM. (c) Schematic of the flow channel connected to two syringes by tubes. The size of the small stainless-steel piece in the channel is indicated. (d) An example of the experimental data detected by the SPM. When the sample solution was at rest, the measured force was close to 0. When the sample solution was flowing, a cantilever attached to the SPM detected the drag forces.

The cantilever was held by a microcell of the SPM, which was attached to a probe cartridge as shown in Figs. 2(a) and 2(b). The probe cartridge was inserted to a probe head [Fig. 2(c)]. The microcell consists of glass window and metal part that allows the laser beam of the SPM to pass through the glass window towards the probe. Figure 2(d) shows a lateral view of the sample stage. The bottom face of the microcell was attached horizontally to the flow surface, at a 2.8 mm height

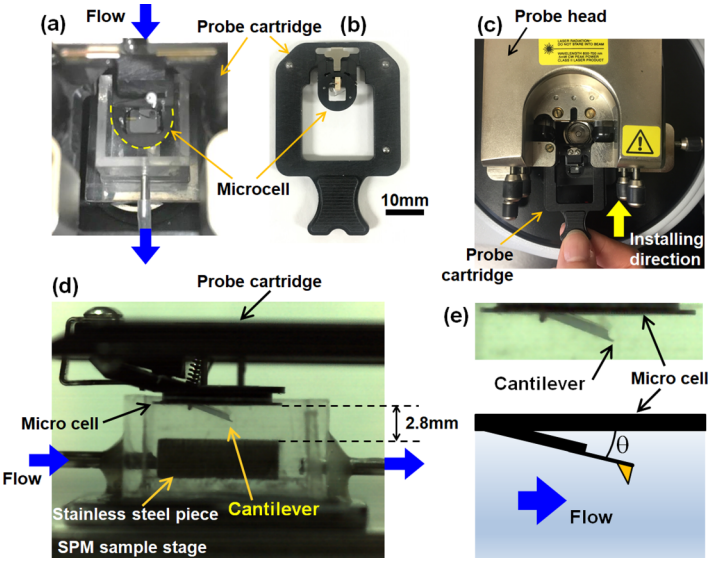

FIG. 2. (a) Top view of the flow channel where the microcell was immersed. (b) The probe cartridge holding the microcell. (c) The probe head of the SPM where the probe cartridge was mounted. (d) The lateral view of the sample stage. The cantilever probe was positioned in the middle of the channel. (e) A close-up image and an illustration of the cantilever. The cantilever was immersed in the flow at an approximate angle $\theta = 15^{\circ}$.

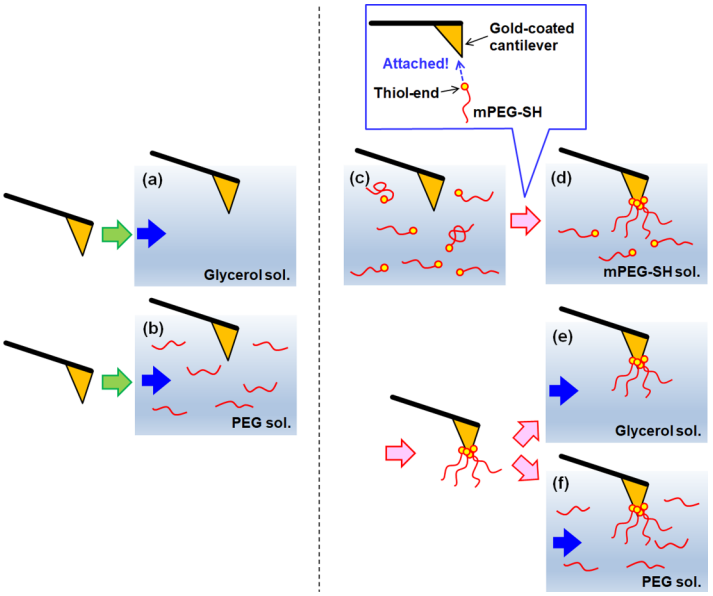

FIG. 3. Schematic illustration of the experimental procedure. A cantilever with the original gold-coated probe was positioned in flowing solutions of (a) glycerol and (b) PEG. The cantilever was further immersed in a mPEG-SH solution (c) to attach thiol-end to the gold-coated probe (d). The mPEG-SH-coated cantilever probe was further immersed in (e) glycerol and (f) PEG solutions.

measured from the top surface of the stainless-steel piece. Figure 2(e) shows a close-up image and the illustration of the cantilever. Since the cantilever dimensions are very small, we cannot see the probe itself in the image. The cantilever was held by the microcell at an angle θ of approximately 15°. The cantilever bows slightly when a force is applied, and this movement is detected through the displacement of the laser beam. The signal from the SPM was measured by an oscilloscope (WaveAce 1001: Teledyne LeCroy). When the sample solution was at rest, the oscilloscope did not detect any force. However, when the sample solution was flowing through the channel, the oscilloscope detects a drag force [Fig. 1(d)]. The increase of the force measured by the probe was analyzed to discuss polymer-fluids interactions and polymer-polymer interactions.

The drag forces were measured at several conditions as shown in Fig. 3. First, the originally gold-coated cantilever probe was used to measure the drag forces in flows of glycerol and PEG solutions [Figs. 3(a) and 3(b)]. Next, we compared drag forces on the original cantilever with that measured on a polymer-bonded cantilever. To prepare the polymer-bonded probe, the cantilever with the original gold coating was sunk in a 1 wt% mPEG-SH solution for 2 h to attach the thiol group via coordinate bonding [Figs. 3(c) and 3(d)]. Previously, we have tested variations on the soaking time of the cantilever from 30 min to 48 h, but the obtained results became constant after a 2 h period. The cantilever was slowly pulled up from the mPEG-SH solution and positioned in the flow channel. The polymer-bonded cantilever with mPEG-SH was used to detect drag forces in the flows of glycerol and PEG solutions [Figs. 3(e) and 3(f)].

To confirm that the adsorbed mass of mPEG-SH was constant after 2 h, and to estimate the number of mPEG-SH molecules on the gold-coated probe, we have used a quartz crystal microbalance (QCM, QCM922A, SEIKO EG&G CO.), with a fundamental resonance frequency of 9 MHz. The diameter of the piezoelectrically active area was 5 mm, which was placed in the flow cell. During the experiments, pure water was injected into the flow cell at a constant flow rate of 50 μL/min for about 15 min to obtain the baseline. The solution was then changed to the 1 wt% solution mPEG-SH, injected at the same flow rate for 2 h.

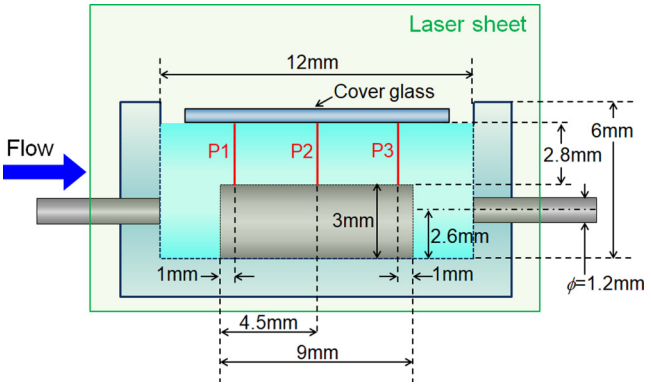

FIG. 4. Schematic illustration of the cross-sectional area of the flow channel. The stainless-steel piece helped to stabilize the flow, producing uniform flow fields at the inlet.

C. Velocity profile measurements in a flow channel

Prior to the previously described experiments, we measured the velocity profiles to certify that the laminar flow was fully developed. The flows were visualized and the velocity profiles were measured using the particle tracking velocimetry method (PTV).

Figure 4 shows the lateral view of the flow channel. The inside dimensions of the channel were 12 mm width, 12 mm depth, and 6 mm high. The dimensions of the stainless-steel piece used to stabilize the flow were 9 mm width, 12 mm depth, and 3 mm high. The sample solutions were injected into the flow channel through the pipe. The chosen test area was that above the stainless-steel piece. As described in the previous section, since the microcell covered the flow surface during the SPM experiments [Fig. 2(d)], a cover glass was set to cover the flow surface during the flow visualization to realize similar velocity fields (Fig. 4). The bottom surface of the cover glass was placed 2.8 mm above the top surface of the stainless-steel piece. The cross-sectional area of the testing section was $2.8 \times 12\,\mathrm{mm}^2$. The center line of the channel was illuminated by a laser sheet with a thickness of 1 mm. Polystyrene particles, with a diameter of 6.83 μm, were seeded in the sample solutions to calculate the velocity profiles by PTV method. The velocity profiles were obtained in the normal direction of the channel at three streamwise positions, P1, P2, and P3, located at 1 mm, 4.5 mm, and at 8 mm, respectively, measured from the top-left corner of the stainless-steel piece.

III. RESULTS AND DISCUSSIONS

A. Velocity profiles in the flow

The velocity profiles measured at the positions P1, P2, and P3 in the channel are shown in Fig. 5. Figure 5(a) shows the velocity profile for the 22 wt% glycerol solution, and Fig. 5(b) shows the same results for the 35 wt% glycerol solution, at the flow rate of 4 ml/min. Reynolds number, $\mathrm{Re_m}$ [-], for each solution was obtained via the following equation:

$$\mathrm{Re_m} = \frac{\rho V_\mathrm{m} D_\mathrm{H}}{\eta}. \tag{2}$$

Here, $\rho[\mathrm{kg/m^3}]$ is the solution density, V_m [m/s] is mean velocity, calculated by dividing the flow rates by the cross-sectional area at P2, D_H [m] is the hydraulic diameter of the channel (=4.54 mm), and η [Pa.s] is the viscosity of each solution. The $\mathrm{Re_m}$ found for the 22 wt% glycerol solution was 5.08, and 4.09 for the 35 wt% solution. In both cases, the velocity profile at each streamwise position was almost the same. We also compared the velocity profiles normalized by the mean velocity, V_m,

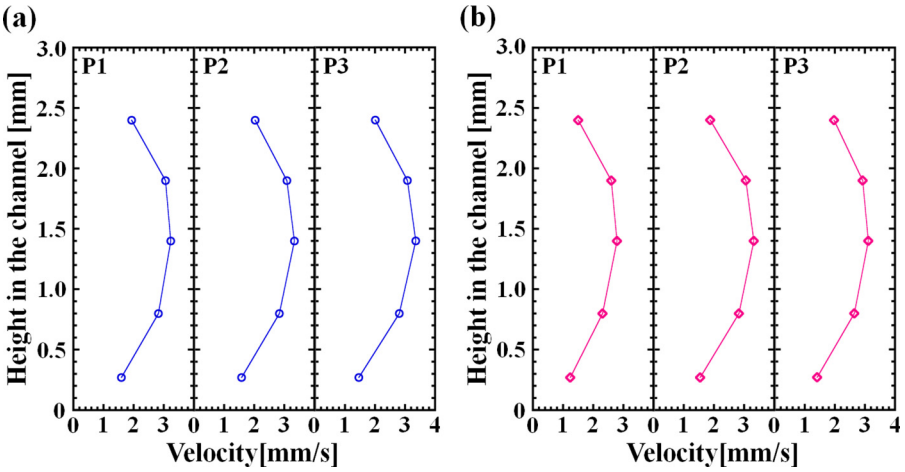

FIG. 5. Local velocity profiles measured at the positions P1, P2, and P3 in 22 wt% and 35 wt% glycerol solutions. The flow rate was 4 ml/min.

as seen in Fig. 6. In the figure, the theoretical velocity profile of the fully-developed laminar flow of Newtonian fluids in a duct with an aspect ratio of 0.233 [49] is plotted (solid line). From this, it is found that the experimentally obtained velocity profiles are in well agreement with the theoretical model, at any Reynolds number from 2.04 to 8.24, proving that the flow is fully developed at the test section in the present study. Heaton *et al.* [50] reported the entry length, L_x [m], of Newtonian fluid as follows:

$$L_x = \frac{D_H \mathrm{Re_m}}{20}. \tag{3}$$

From this, the entry length can be estimated as being 1.15 mm in the case when $\mathrm{Re_m} = 5.08$. In this study, the largest $\mathrm{Re_m}$ was 8.24. Even in this condition, the entry length is at most about 1.87 mm. Thus, the velocity field was fully developed at P2 in any condition.

The probe of the cantilever was then immersed in the center of the channel at a position close to P2, and at a height close to 1.4 mm, measured from the top surface of the stainless-steel piece.

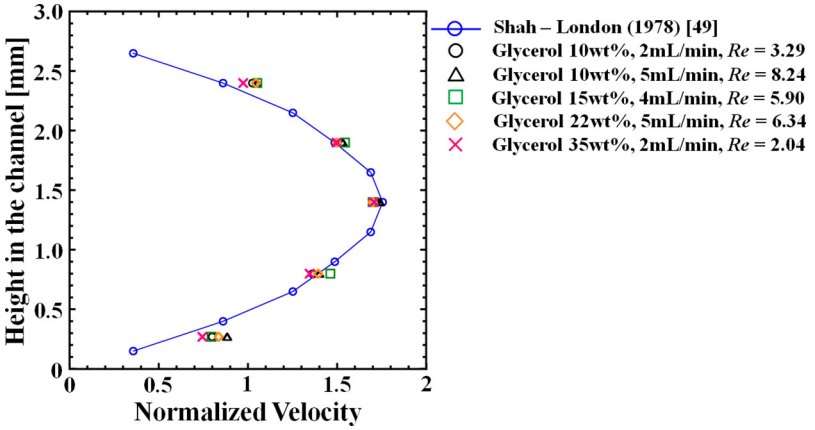

FIG. 6. Normalized velocity profile for each glycerol solution.

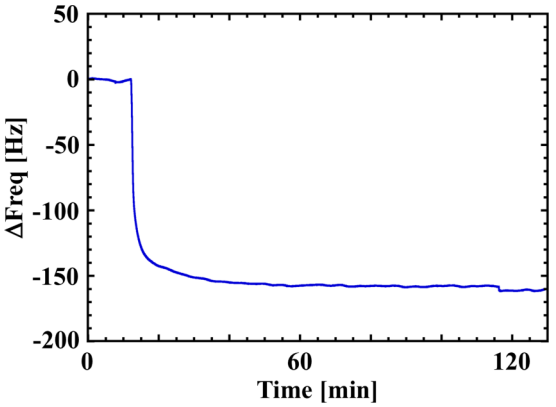

FIG. 7. An example of the change in the resonant frequency ΔFreq during a QCM experiment.

Thus, we used the velocity at the height of 1.4 mm at the position P2 for the following analysis. Since the velocity profiles were fully developed as shown in Figs. 5 and 6, the velocity gradient in any direction is almost zero at the middle height. Therefore, lift forces on the probe can be neglected. The velocity profiles shown in Figs. 5 and 6 were obtained without the cantilever, therefore, they may be varied in the cantilever presence. However, we can assume the change in the velocity fields to be small because the equivalent diameter of the cantilever probe is less than 0.26% of the channel height, and its width is only 0.25% of the channel width. Therefore, we used the velocity at the height of 1.4 mm, at the position P2, as the actual characteristic velocity.

B. QCM measurements and distance between two mPEG-SH attached to the probe

The adsorption mass of mPEG-SH on the gold surface of the probe accumulated for 2 h was measured by QCM experiments. The mass of mPEG-SH adsorbed on the gold sensor was calculated by the frequency change in the sensor oscillation, ΔFreq [Hz], by using the Sauerbrey equation [51].

$$\Delta\mathrm{Freq} = -\frac{2}{\sqrt{\mu_q \rho_q}} \frac{\mathrm{Freq}^2}{\mathrm{n_{ot}}} \frac{\Delta m}{A}, \tag{4}$$

where Δm[ng/cm^2] is the adsorbed mass, A[m^2] is the piezoelectric quartz sensor area, Freq [Hz] is the fundamental resonance frequency, $\mathrm{n_{ot}}$ [-] is the overtone number, μ_q[kg/m $\cdot$ s^2] is the shear modulus of the quartz, and ρ_q[kg/m^3] is the density of quartz. Here, $\mathrm{n_{ot}} = 1$.

An example of the change in the resonant frequency ΔFreq during an experiment is shown in Fig. 7. The adsorption of mPEG-SH starts very quickly after the injection of the 1 wt% mPEG-SH solution. The ΔFreq reaches a constant value of about $\Delta\mathrm{Freq} = -160$ Hz after 2 h. According to Eq. (4), the mass of mPEG-SH adsorbed on the gold surface is 880 ng/cm^2, higher than the 220 ng/cm^2 value suggested in previous studies [52]. We considered the ΔFreq obtained with a QCM coupled with the effects of the viscoelasticity of the mPEG-SH itself and the viscoelasticity of the mPEG-SH solution around the sensor as suggested in the previous studies [52,53]. Therefore, ΔFreq became lower than the expected value. However, the most important result obtained here is the mPEG-SH adsorbed mass on the gold surface of the sensor became constant after 2 h.

Here we assume that the mPEG-SH grafting distance, which is the spacing between two polymers, as being 3.9 nm, obtained by Surface Plasmon Resonance [52]. According to the previous study, which used the same mPEG-SH of the present study, mPEG-SH was grafted on a gold surface with the distance of 3.9 ± 0.4 nm. In addition, the grafted mPEG-SH was extended as the length of 18.7 ± 2.7 nm [52]. These values were referred to calculate the drag force of mPEG-SH in flows, to discuss experimental data of the following section.

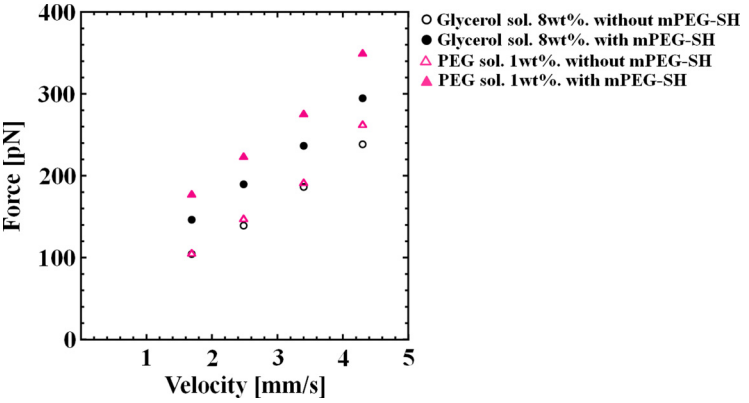

FIG. 8. Forces detected by the naked probe cantilever and by the polymer-bonded cantilever, in flowing solutions at several velocities. The viscosities of the 8 wt% glycerol solution and of the 1 wt% PEG solution are the same.

C. Force measurements in the flow

Figure 8 shows the forces detected by the cantilever in flows of an 8 wt% glycerol solution and a 1 wt% PEG solution, at several velocities. The viscosity of the glycerol and PEG solutions was the same, as shown in Tables I and II. The force measured by the naked cantilever probe in the 8 wt% glycerol solution is almost the same as the force measured in the 1 wt% PEG solution. The schematic image of this comparison is shown in Figs. 3(a) and 3(b). When the mPEG-SH molecules are attached to the cantilever probe, the detected force is increased at any velocity in the glycerol solution. The increase in the detected force measured by the polymer-bonded cantilever is also observed in the flow of the 1 wt% PEG solution. The variation on the force detected by the cantilever with or without mPEG-SH, in the flow of the PEG solution, is larger than that in the glycerol solution at a corresponding velocity. As illustrated in Figs. 3(e) and 3(f), we attribute the increase of the force measured by the polymer-bonded cantilever in the PEG solution, when compared to the glycerol solution, to be caused by interactions between the mPEG-SH and the PEG of the solution. The PEG molecules dissolved in the flowing fluid touch the mPEG-SH bonded to the cantilever probe, increasing the drag force. In the present study, we called this interaction as a polymer-polymer interaction.

To verify the validity of the results, we calculated the drag coefficient, C_{d} [-], of the cantilever probe using the following expression:

$$C_d = \frac{F}{\frac{1}{2}\rho V^2 \frac{\pi}{4} d^2}. \tag{5}$$

Here, F [N] is the force applied to the cantilever, ρ[kg/m^3] is the density of each solution, V [m/s] is the velocity at the location (middle height, position P2), and d [m] is the equivalent diameter of the probe. The front view of the probe has an isosceles triangular shape with a 12-μm base and a 7-μm height with an apex angle of 2α [°] [Fig. 12(e)]. Thus, the equivalent diameter d [m] of the probing area is 7.4 μm. Figure 9 shows the C_{d} values found for the naked cantilever probe, plotted as a function of the Reynolds number, Re. In the figure, Re was calculated using the local velocity, V, and the equivalent diameter of the probe, d, as described in Eq. (6):

$$\mathrm{Re} = \frac{\rho V d}{\eta}. \tag{6}$$

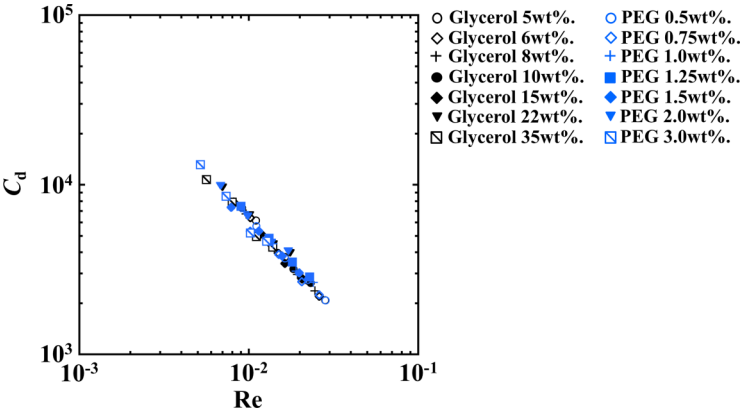

FIG. 9. C_d-Re plot for the naked cantilever probe in glycerol and PEG solutions.

In the case of a naked cantilever probe, C_d should depend only on Re. From the figure, it is found that C_d is not affected by the solute, the concentration, or the solution viscosity. Thus, the C_d plot as a function of Re, for the naked cantilever, verifies the validity of our measurements.

We compared the C_d values of the naked cantilever probe with those of the polymer-bonded cantilever probe. Figure 10(a) shows the C_d values of the considered probes in glycerol solutions, and Fig. 10(b) shows those in PEG solutions. The C_d of the polymer-bonded probe was higher compared to that of the naked one, in both solutions. The increase of C_d, namely, the ΔC_d indicated in the figure, is higher for PEG than for glycerol solutions. We attribute the ΔC_d increase in the flowing PEG solution to be caused by the interactions between polymers bonded at cantilever probe and polymers in the flow. In other words, this difference is caused by polymer-polymer interactions.

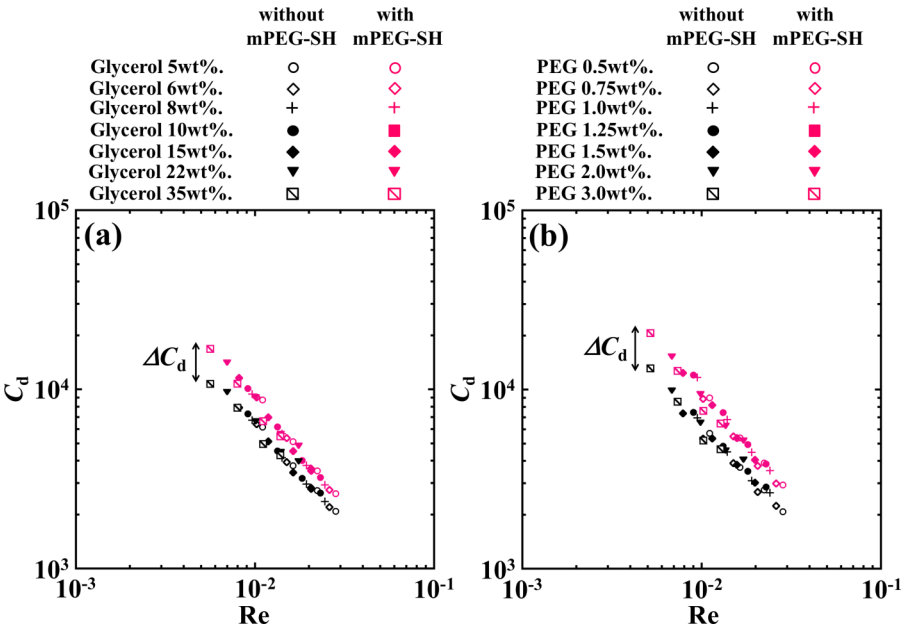

FIG. 10. Comparison between the C_d values of a naked cantilever probe, and a polymer-bonded cantilever probe (a) in glycerol solutions and (b) in PEG solutions.

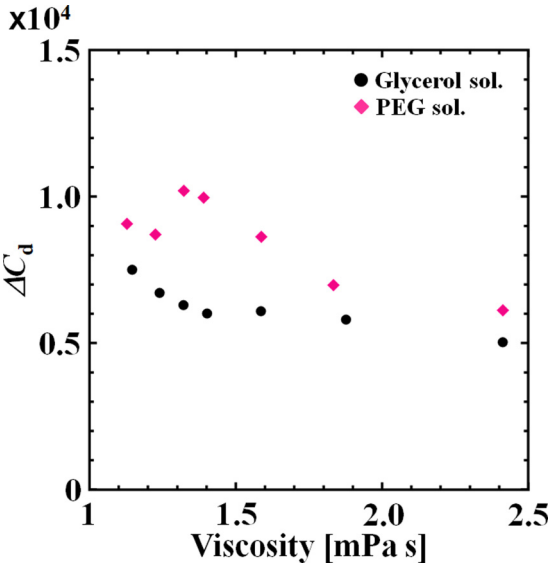

FIG. 11. The ΔC_d in each solution plotted as a function of their viscosities.

The ΔC_d in each solution was plotted as a function of their viscosities and shown in Fig. 11. From the figure, the polymer-polymer interaction was clearly observed, affecting the force measured by the polymer-bonded probe in flowing PEG solutions.

D. Discussion on the polymer conformation and the drag force due to polymers

To consider the increase of the C_d values, the drag force due to polymers attached on the cantilever probe was calculated. For that, we first predict how the attached polymers are deformed in the flow, and then we calculate the drag force due to the deformed molecules.

For the first part, we refer to the index φ described in Eq. (1). We calculated φ for each attached polymer in flowing glycerol solutions. To do so, the force f [N] acting on a single polymer needs to be identified. Here, we derived f [N] via experimental data using the following procedure.

Firstly, we calculated increase of the torque applied to a cantilever due to attached polymers, $\Delta F \times L$ [N.m]. Here, ΔF [N] is the increase of the detected force, calculated as the difference between the forces on the polymer-bonded probe and the naked probe, at an equal flow rate and solution. L [m] is the length of the cantilever beam, that is 100 μm [Fig. 12(b)]. Then, $\Delta F \times L$ equals the summation of torque due to each single polymer attached on the probe:

$$\Delta FL = \left(\sum_{i=1}^{n} f l_i \times \cos\alpha \right) \times 2 \times \cos\theta. \tag{7}$$

The cantilever was immersed in the flow with an angle of $\theta = 15^\circ$ [Fig. 12(a)]. As shown in Figs. 12(b)–12(d), n [-] is the number of bonded polymers in a line along the probe, and l_i [m] is the length between the upper edge of the probe and the position where the polymer attached. In the calculation, we took into account only the polymers that attached to the edge of the probe, and the reason for this is explained in the next paragraph. As shown in the same figure, only these polymers were subjected to the flow. In addition, since the probe is V-shaped, the torque must be calculated for the both sides of the probe [Figs. 12(c)–12(e)], explaining the factor "× 2" in Eq. (7). It is also required to take into account the apex angle 2α for the calculation of the torque applied in

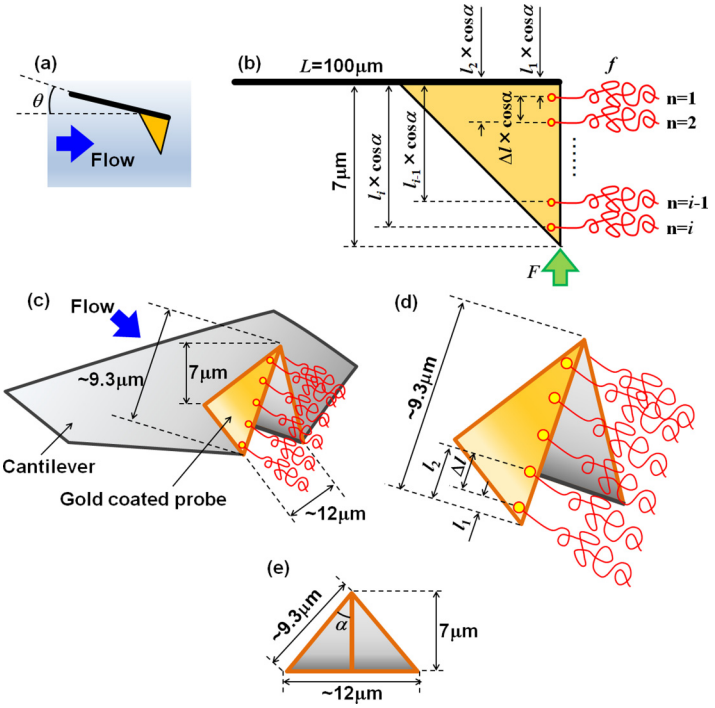

FIG. 12. (a) Schematic of the cantilever, tilted with an angle $\theta = 15^\circ$ to the flow. (b) Schematic of the mPEG-SH attached to the gold-coated probe of the cantilever from the lateral view. (c) Upside-down image of the cantilever to illustrate the V-shaped probe, where mPEG-SH molecules attach to its both lateral sides. (d) Close-up figure of the probe to indicate l_i and Δl along the edge. (e) Close-up figure of the probe from the downstream view showing the apex angle.

the same axis. Here, the summation of the right side of Eq. (7) results in Eq. (8):

$$\sum_{i=1}^{n} f l_i \times \cos\alpha = f \times \Delta l \times \frac{1}{2}\mathrm{n(n-1)} \times \cos\alpha, \tag{8}$$

where Δl [m] is the grafting distance, which is 3.9 nm as described in the Sec. III B. In addition, the length of the V-shaped edge was calculated as being about 9.3 μm. Therefore, the calculated number of bonded polymer molecules at the edge on the probe, n, is approximately 2380. Combining Eqs. (7) and (8), f was obtained and used to calculate φ. The φ value for a single polymer molecule in glycerol solutions was between 0.02 and 0.07. The value of φ increased with the flow rate, as well as with the glycerol concentration. Since φ is less than 1, polymers are not deformed only by the effects of the flow. In the present condition, the steric repulsion effect between each mPEG-SH molecule attached to the probe causes the stretching of the polymers themselves [52]. To estimate the contribution of each polymer molecule in the flow on ΔF, we assume here a stem and ellipsoidal-flower shape as the mPEG-SH conformation. We suggest the ellipsoidal-flower shape because of the short grafting distance, so that the flower part does not have enough space to keep its spherical shape. In this manner, we tried to simplify the shape of the polymers deformed by the steric repulsive effect.

The reason why only the polymers at the rear edge were considered in the calculation is related to a boundary layer developed on the probe during the flow. As shown in Figs. 12(c) and 12(d), the flow sweeps the probe from its oblique side towards the V-shaped edge. Therefore, a laminar boundary layer develops from the front edge of the oblique side of the probe. According to previous calculations [54], the laminar boundary layer on the wall of the probe is much thicker than the

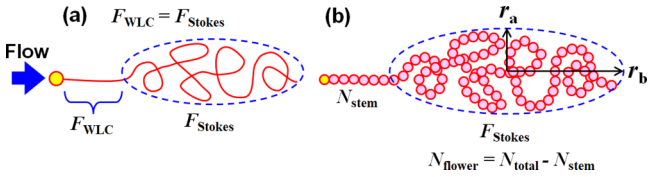

FIG. 13. (a) Force balance between the stem part and the ellipsoidal-flower part. (b) Close-up figure of the polymer, focusing on the number of monomers.

polymer size. Therefore, even in the case where the polymers attached to the oblique side of the probe are fully extended, the velocity at this position is only 0.3% of the characteristic velocity. Therefore, the polymers attached to the side walls of the probe are not subjected to the main flow, except those at the rear edge where the flow turns around the edge.

For the second step, that focused on predicting the conformation of the molecules, it is required to calculate the number of monomers in the stem part, N_{stem} [-], and in the ellipsoidal-flower part, N_{flower} [-] (Fig. 13). Here, the total number of monomers in a polymer, N_{total}, is given by the summation $N_{\mathrm{total}} = N_{\mathrm{stem}} + N_{\mathrm{flower}}$. If we focus on a single polymer, there is a force balance between the stem part and the ellipsoidal-flower part. Therefore, we calculated the force due to the stem part, F_{WLC} [N], by using the worm like chain (WLC) model. This model was proposed to describe the force curve to stretch a single polymer molecule, as follows [24,27]:

$$F_{\mathrm{WLC}} = \frac{k_{\mathrm{B}}T}{l_{\mathrm{op}}}\left[\frac{1}{4(1 - x/L_{\mathrm{total}})} + \frac{x}{L_{\mathrm{total}}} - \frac{1}{4}\right], \tag{9}$$

where l_{op} is the persistent length, the same as in Eq. (1), x [m] is the extension length, and L_{total} [m] is the contour length. Here, $x = N_{\mathrm{stem}} \times l_{\mathrm{op}}$, and $L_{\mathrm{total}} = N_{\mathrm{total}} \times l_{\mathrm{op}}$. The force due to the ellipsoidal-flower part, F_{stokes} [N], was calculated by using the stokes drag model [55,56]:

$$F_{\mathrm{stokes}} = 6\pi\eta r_a \left\{1 - \frac{1}{5}\left(1 - \frac{r_b}{r_a}\right)\right\} V. \tag{10}$$

Here, r_a [m] is the radius of the minor axis and r_b [m] is the radius of the major axis, both of the ellipsoidal-flower part [Fig. 13(b)]. We assume that $r_a = 1.95 \times 10^{-9}$ m, the half of the grafting distance, which is a constant value. The F_{WLC} and F_{stokes} should balance each other in a polymer molecule during the flow to keep the stem and flower shape steady. Therefore, the force balance between F_{WLC} and F_{stokes} was used to obtain r_b at each velocity and solution viscosity. Then we estimated the number of monomers in the ellipsoidal-flower part by $r_b = a(N_{\mathrm{flower}})^{3/5}$, where a[m] $= 3.8 \times 10^{-10}$ m is the diameter of a monomer in PEG. The number of monomers in the stem part was obtained by $N_{\mathrm{stem}} = N_{\mathrm{total}} - N_{\mathrm{flower}}$. We have also calculated the total length of each polymer during each flow, which is the sum of the lengths of stem and ellipsoidal-flower parts: $a \times N_{\mathrm{stem}} + 2r_b$. The calculated lengths were about 31 to 37 nm at each condition, which is reasonably close to the length of the grafted PEG, of 18.7 ± 2.7 nm, measured by SPR [52]. The difference on the lengths was considered to be caused by the effects of the flow. Therefore, we conclude that our assumption of deformed polymers, in the stem and ellipsoidal-flower shape conformations, calculated by the grafting distance of 3.9 nm [52], was reasonable. Then, we assume the force due to the ellipsoidal-flower part, F_{stokes} [N], obtained by Eq. (10), to be the drag force due to a single deformed polymer, f_{single} [N]:

$$f_{\mathrm{single}} = F_{\mathrm{stokes}}. \tag{11}$$

Finally, we can compare the left side and the right side in Eq. (12):

$$\Delta F = \frac{\left(\sum_{i=1}^{\mathrm{n}} f_{\mathrm{single}} l_i \times \cos\alpha\right) \times 2 \times \cos\theta}{L}, \tag{12}$$

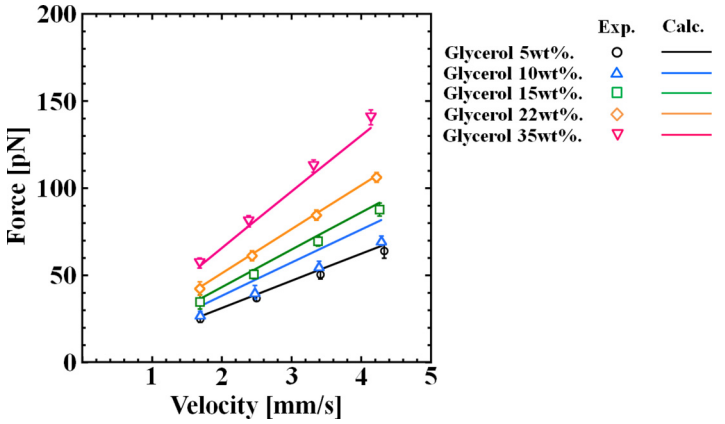

FIG. 14. Comparison of ΔF on the left and the right side of Eq. (12). The former was obtained experimentally (Exp.), and the latter was obtained by calculations (Calc.). ΔF is the difference between the force measured by the polymer-bonded probe cantilever and the force measured by a naked probe cantilever. To eliminate the measurement noise, the force measured by each cantilever was fitted by least squares prior to the calculation of ΔF. Experiments were done with multiple cantilevers, therefore the experimental value is indicated with the error bar.

where ΔF is the above-described experimental value in Eq. (7), and the right side is obtained by the previously discussed calculation. Figure 14 shows the comparison of ΔF and the right side of Eq. (12). The force due to bonded polymers measured experimentally, ΔF, are reasonably close to the force calculated based on a stem and ellipsoidal-flower model in flowing glycerol solutions. It was verified in Fig. 14 that the tendency of the force to increase with the velocities was surprisingly the same. Therefore, we consider that our assumption of the polymer deformation, and the force due to a single polymer, is reasonable to describe the polymer properties in flowing solutions.

IV. CONCLUSION

In this study, we conducted the measurements of the drag force due to synthetic polymers in a flow using a SPM. A mPEG-SH-bonded cantilever held by the SPM was immersed in flows of glycerol and PEG solutions. The cantilever detects the extra force due to polymer-fluids and polymer-polymer interactions, quantified by the drag coefficients of the cantilever probe. To confirm the origin of the drag force, the conformation of the mPEG-SH polymer bonded at the cantilever probe was predicted by the φ index. In the present conditions, φ was sufficiently small, preventing the polymer to be deformed only by the flow effects. However, since the grafting distance was small, it is reasonable to consider that each polymer was stretched due to the steric repulsive effect. We assumed that the polymer conformation was the stem and ellipsoidal-flower types and calculated the drag force of each mPEG-SH molecule based on the Stokes' drag of the flower part. The drag force due to the attached polymers, obtained by the calculations, was close to the force measured by experiments. Thus, our assumption of deformed polymers, in the stem and ellipsoidal-flower shape conformations, calculated by the grafting distance of 3.9 nm was considered to be reasonable. To the best of our knowledge, this trial is the first to measure the drag force of synthetic polymers in a flow. The method proposed in this study can be applied to detect polymer conformations in a flow. We believe the findings obtained in the present study will contribute to clarify many topics, such as the complex behavior of dilute polymer solutions, and the biopolymer conformation in biological flowing fluids.

ACKNOWLEDGMENTS

The present study was financially supported by a Grant-in-Aid for Young Scientists (A) (Project No. 15H05552) and a Grant-in-Aid for Scientific Research (B) (Project No. 19H02497), from the Japan Society for the Promotion of Science (JSPS KAKENHI).

[1] F. T. Pinho and J. H. Whitelaw, Flow of non-Newtonian fluids in a pipe, J. Non-Newtonian Fluid Mech. **34**, 129 (1990).
[2] T. Wei and W. W. Willmarth, Modifying turbulent structure with drag-reducing polymer additives in turbulent channel flows, J. Fluid Mech. **245**, 619 (1992).
[3] C. Wagner, Y. Amarouchene, P. Doyle, and D. Bonn, Turbulent-drag reduction of polyelectrolyte solutions: Relation with the elongational viscosity, Europhys. Lett. **64**, 823 (2003).
[4] M. D. Graham, Drag reduction and the dynamics of turbulence in simple and complex fluids, Phys. Fluids **26**, 101301 (2014).
[5] A. Japper-Jaafar, M. P. Escudier, and R. J. Poole, Turbulent pipe flow of a drag-reducing rigid "rod-like" polymer solution, J. Non-Newtonian Fluid Mech. **161**, 86 (2009).
[6] R. Hidema, H. Suzuki, S. Hisamatsu, Y. Komoda, and H. Furukawa, Effects of the extensional rate on two-dimensional turbulence of semi-dilute polymer solution flows, Rheol. Acta, **52**, 949 (2013).
[7] R. Hidema, H. Suzuki, S. Hisamatsu, and Y. Komoda, Characteristic scales of two-dimensional turbulence in polymer solutions, AIChE J. **60**, 1854 (2014).
[8] R. Hidema, H. Suzuki, I. Murao, S. Hisamatsu, and Y. Komoda, Effects of extensional rates on anisotropic structures and characteristic scales of two-dimensional turbulence in polymer solutions, Flow Turbulence Combust. **96**, 227 (2016).
[9] R. Hidema, I. Murao, Y. Komoda, and H. Suzuki, Effects of the extensional rheological properties of polymer solutions on vortex shedding and turbulence characteristics in a two-dimensional turbulent flow, J. Non-Newtonian Fluid Mech. **254**, 1 (2018).
[10] A. Groisman and V. Steinberg, Elastic turbulence in a polymer solution flow, Nature **405**, 53 (2000).
[11] L. E. Rodd, T. P. Scott, D. V. Boger, J. J. Cooper-White, and G. H. McKinley, The inertio-elastic planar entry flow of low-viscosity elastic fluids in micro-fabricated geometries, J. Non-Newtonian Fluid Mech. **129**, 1 (2005).
[12] L. E. Rodd, J. J. Cooper-White, D. V. Boger, and G. H. McKinley, Role of the elasticity number in the entry flow of dilute polymer solutions in micro-fabricated contraction geometries, J. Non-Newtonian Fluid Mech. **143**, 170 (2007).
[13] Y. Jun and V. Steinberg, Elastic turbulence in a curvilinear channel flow, Phys. Rev. E **84**, 056325 (2011).
[14] A. Lanzaro and X.-F. Yuan, A quantitative analysis of spatial extensional rate distribution in nonlinear viscoelastic flows, J. Non-Newtonian Fluid Mech. **207**, 32 (2014).
[15] T. Sridhar, V. Tirtaatmadja, D. A. Nguyen, and R. K. Gupta, Measurement of extensional viscosity of polymer solutions, J. Non-Newtonian Fluid Mech. **40**, 271 (1991).
[16] G. H. McKinley and T. Sridhar, Filament stretching rheometry of complex fluids, Annu. Rev. Fluid Mech. **34**, 375 (2002).
[17] V. Sharma, S. J. Haward, J. Serdy, B. Keshavarz, A. Soderlund, P. Threlfall-Holmesf, and G. H. McKinley, The rheology of aqueous solutions of ethyl hydroxy-ethyl cellulose (EHEC) and its hydrophobically modified analogue (hmEHEC): Extensional flow response in capillary break-up, jetting (ROJER) and in a cross-slot extensional rheometer, Soft Matter **11**, 3251 (2015).
[18] F. Del Giudice, S. J. Haward, and A. Q. Shen, Relaxation time of dilute polymer solutions: A microfluidic approach, J. Rheology **61**, 327 (2017).
[19] P. C. Sousa, E. J. Vega, R. G. Sousa, J. M. Montanero, and M. A. Alves, Measurement of relaxation times in extensional flow of weakly viscoelastic polymer solutions, Rheol. Acta **56**, 11 (2017).
[20] R. Hidema, T. Shiraki, Y. Tanino, Y. Komoda, and H. Suzuki, Extensional viscosity of low viscous polymer solutions measured by pressure drops in abrupt contraction channels, Nihon Reoroji Gakkaishi (J. Soc. Rheol. Japan) **46**, 13 (2018).

[21] C. Ortiz and G. Hadziioannou, Entropic elasticity of single polymer chains of poly(methacrylic acid) measured by atomic force microscopy, Macromolecules **32**, 780 (1999).
[22] M. Rief, M. Gautel, F. Oesterhelt, J. M. Fernandez, and H. E. Gaub, Single molecule force spectroscopy on polysaccharides by atomic force microscopy, Science **275**, 1295 (1997).
[23] F. Oesterhelt, M. Rief, and H. E. Gaub, Single molecule force spectroscopy by AFM indicates helical structure of poly(ethylene-glycol) in water, New J. Phys. **1**, 6 (1999).
[24] K. Nakajima and T. Nishi, Nanoscience of single polymer chains revealed by nanofishing, Chem. Record **6**, 249 (2006).
[25] F. Kienberger, V. Ph. Pastushenko, G. Kada, H. J. Gruber, C. Riener, H. Schindler, and P. Hinterdorfer, Static and dynamical properties of single poly(ethylene glycol) molecules investigated by force spectroscopy, Single Mol. **1**, 123 (2000).
[26] C. Bustamante, Entropic elasticity of λ-phage DNA, Science **265**, 1599 (1994).
[27] M. I. Giannotti and G. J. Vancso, Interrogation of single synthetic polymer chains and polysaccharides by AFM-based force spectroscopy, ChemPhysChem **8**, 2290 (2007).
[28] M. Hinczewski and R. R. Netz, Anisotropic hydrodynamic mean-field theory for semiflexible polymers under tension, Macromolecules **44**, 6972 (2011).
[29] M. Radiom and M. Borkovec, Influence of ligand-receptor interactions on force-extension behavior within the freely jointed chain model, Phys. Rev. E **96**, 062501 (2017).
[30] M. S. Z. Kellermayer, S. B. Smith, H. L. Granzier, and C. Bustamante, Folding-unfolding transitions in single titin molecules characterized with laser tweezers, Science **276**, 1112 (1997).
[31] Z. N. Scholl, Q. Li, and P. E. Marszalek, Single molecule mechanical manipulation for studying biological properties of proteins, DNA, and sugars, WIREs Nanomed Nanobiotechnol. **6**, 211 (2014).
[32] N. B. Holland, T. Hugel, G. Neuert, A. Cattani-Scholz, C. Renner, D. Oesterhelt, L. Moroder, M. Seitz, and H. E. Gaub, Single molecule force spectroscopy of azobenzene polymers: Switching elasticity of single photochromic macromolecules, Macromolecules **36**, 2015 (2003).
[33] M. I. Giannotti, I. Cabeza de Vaca, J. M. Artés, F. Sanz, V. Guallar, and P. Gorostiza, Direct measurement of the nanomechanical stability of a redox protein active site and its dependence upon metal binding, J. Phys. Chem. **119**, 12050 (2015).
[34] H. Li, W. Zhang, W. Xu, and X. Zhang, Hydrogen bonding governs the elastic properties of poly(vinyl alcohol) in water: Single-molecule force spectroscopic studies of PVA by AFM, Macromolecules **33**, 465 (2000).
[35] B. J. Haupt, T. J. Senden, and E. M. Sevick, AFM evidence of Rayleigh instability in single polymer chains, Langmuir **18**, 2174 (2002).
[36] L. Grebikova, M. Radiom, P. Maroni, A. D. Schlüter, and M. Borkovec, Recording stretching response of single polymer chains adsorbed on solid substrates, Polymer **102**, 350 (2016).
[37] Z. Li, B. Zhang, Y. Song, Y. Xue, L. Wu, and W. Zhang, Single molecule study on polymer−nanoparticle interactions: The particle shape matters, Langmuir **33**, 7615 (2017).
[38] F. Brochard-Wyart, T. H. Hervet, and P. Pincu, Unwinding of polymer chains under forces or flows, Europhys. Lett. **26**, 511 (1994).
[39] F. Brochard-Wyart, Polymer chains under strong flows: Stems and flowers, Europhys. Lett. **30**, 387 (1995).
[40] R. Rzehak, W. Kromen, T. Kawakatsu, and W. Zimmermann, Deformation of a tethered polymer in uniform flow, Eur. Phys. J. E **2**, 3 (2000).
[41] C. A. Lueth and E. S. G. Shaqfeh, Experimental and numerical studies of tethered DNA shear dynamics in the flow-gradient plane, Macromolecules **42**, 9170 (2009).
[42] T. Y. Lin, A. Saadat, A. Kushwaha, and E. S. G. Shaqfeh, Effect of length on the dynamics of wall tethered polymers in shear flow, Macromolecules **51**, 254 (2018).
[43] T. T. Perkins, D. E. Smith, R. G. Larson, and S. Chu, Stretching of a single tethered polymer in a uniform flow, Science **268**, 83 (1995).
[44] B. Ladoux and P. S. Doyle, Stretching tethered DNA chains in shear flow, Europhys. Lett. **52**, 511 (2000).
[45] T. Roy, K. Szuttor, J. Smiatek, C. Holm, and S. Hardt, Stretching of surface-tethered polymers in pressure-driven flow under confinement, Soft Matter **13**, 6189 (2017).

[46] J. K. Fisher, M. Ballenger, E. T. O'Brien, J. Haase, R. Superfine, and K. Bloom, DNA relaxation dynamics as a probe for the intracellular environment, Proc. Natl. Acad. Sci. USA **106**, 9250 (2009).
[47] F. Brochard-Wyart, A. Buguin, and P. G. de Gennes, Dynamics of taut DNA chains, Europhys. Lett. **47**, 171 (1999).
[48] Y. Wang, A. Warshawsky, C. Wang, N. Kahana, C. Chevall, and V. Steinberg, Fluorescent ultrahigh-molecular-weight polyacrylamide probes for dynamic flow systems: Synthesis, conformational behavior and imaging, Macromol. Chem. Phys. **203**, 1833 (2002).
[49] R. K. Shah and A. L. London, *Laminar Forced Convection in Ducts* (Academic Press, San Diego, 1978).
[50] H. S. Heaton, W. C. Reynolds, and W. M. Kays, Heat transfer in annular passages. Simultaneous development of velocity and temperature fields in laminar flow, Int. J. Heat and Mass Trans. **7**, 763 (1964).
[51] G. Sauerbrey, Verwendung von schwingquarzen zur wägung dünner schichten und zur mikrowägung, Zeitschrift für Physik **155**, 206 (1959).
[52] R. L. Schoch and R. Y. H. Lim, Non-interacting molecules as innate structural probes in surface plasmon resonance, Langmuir **29**, 4068 (2013).
[53] F. Höök and B. Kasemo, Variations in coupled water, viscoelastic properties, and film thickness of a Mefp-1 protein film during adsorption and cross-linking: A quartz crystal microbalance with dissipation monitoring, ellipsometry, and surface plasmon resonance study, Anal. Chem. **73**, 5796 (2001).
[54] L. Howarth, On the solution of the laminar boundary layer equations, Proc. Roy. Soc. London. Ser. A **164**, 547 (1938).
[55] Y. Magariyama, S. Sugiyama, K. Muramoto, I. Kawagishi, Y. Imae, and S. Kudo, Simultaneous measurement of bacterial flagellar rotation rate and swimming speed, Biophysical J. **69**, 2154 (1995).
[56] J. Happel and H. Brenner, *Low Reynolds Number Hydrodynamics* (Springer, Berlin, 1983).